Dependence of the optical conductivity on the uniaxial and biaxial strains in black phosphorene

C. H. Yang,[1,2] J. Y. Zhang,[1] G. X. Wang,[3] and C. Zhang[2,*]

[1]*School of Physics and Optoelectronic Engineering, Nanjing University of Information Science and Technology, Nanjing 210044, China*
[2]*School of Physics and Institute for Superconducting and Electronic Materials, University of Wollongong, New South Wales 2552, Australia*
[3]*Center for Clean Energy Technology, School of Mathematical and Physical Sciences, University of Technology Sydney, Sydney NSW 2007, Australia*

(Received 26 November 2017; revised manuscript received 2 April 2018; published 12 June 2018)

By using the Kubo formula, the optical conductivity of strained black phosphorene was studied. The anisotropic band dispersion gives rise to an orientation dependent optical conductivity. The energy gap can be tuned by the uniaxial and biaxial strains which can be observed from the interband optical conductivity polarized along the armchair (x) direction. The preferential conducting direction is along the x direction. The dependence of the intraband optical conductivity along the zigzag (y) direction on the Fermi energy and strain exhibits increasing or decreasing monotonously. However, along the x direction this dependence is complicated which originates from the carriers' inverse-direction movements obtained by two types of the nearest phosphorus atom interactions. The modification of the biaxial strain on the energy structure and optical-absorption property is more effective. The imaginary part of the total optical conductivity (Imσ) can be negative around the threshold of the interband optical transition by modifying the chemical potential. Away from this frequency region, Imσ exhibits positive value. It can be used in the application of the surface plasmon propagations in multilayer dielectric structures.

DOI: 10.1103/PhysRevB.97.245408

I. INTRODUCTION

The research on graphene has spurred diverse efforts to investigate other two-dimensional (2D) materials, such as black phosphorene (BP) [1,2] and other more than 600 stable exfoliated 2D materials [3] because of their rich optical, electrical, and mechanical physics and potential applications [4,5]. BP is a 2D direct-gap semiconductor with a honeycomblike structure. It is similar to graphene, but is nonplanar. The carrier's band structure can be obtained by the tight-binding approach [6,7]. In contrast to graphene, the tight binding for BP involves two important parameters, describing the in-plane and out-of-plane nearest-neighbor hoppings, and the second parameter is shown to be largely responsible for the band-gap opening. BP possesses a finite band gap with a predicted band gap of 2 eV [8] which varies with the layer number (layer thickness) [7–9], stacking order [10], the external strain engineering [9,11–13], doping [14,15], and superlattice potential [16]. With the increase of the layer number of BP, the band gap decreases [7–9]. Mechanics strain is an effective means to tune the energy band gap. In the presence of strain, the change of the bond length between the nearest- and the next-nearest atoms leads to the modulation of the hopping energy. The hopping energy is dependent on the strain components for different strain directions. Within the tight-binding model, the dependence of the energy band gap on the strain for single layer BP has been obtained [9]. The analytical band gap variation induced by a general strain has been derived and the maximum (or minimum) strain effect on the band gap can be achieved [12]. Based on the density function theory calculations, the BP shows good stability under tensile strains, while it shows instability under compression strains [13]. Considering potassium doping on the surface of BP, it was found that the band gap was closed completely and the material was tuned from a semiconductor to a band-inverted semimetal. At a critical doping, an emergence of 2D massless Dirac cones has been observed with linear and quadratic energy dispersions along the armchair and zigzag directions, respectively [14,15]. In the presence of the 1D superlattice potential the energy band gap around the Dirac cone has been reduced [16]. These diverse approaches being used to tune the energy gap and energy dispersion provide a high feasibility in the applications of photonic and optoelectronic devices that can operate at different frequencies in BP.

Arising from the structural anisotropy, the most distinctive characteristic of BP from the other 2D materials is its anisotropic properties, which leads to a direction-dependent electronic [10,15,17,18], optical [9–11,18–21], thermal [22–24], and mechanical properties [25]. The electron/hole effective masses along the armchair and zigzag directions at the Γ point have an approximate "8" shape, which indicates the anisotropic nature of the electronic properties because BP has a highly anisotropic band structure around the band gap [10]. The anisotropic electronic mobility and electrical conductance have been investigated by first-principle simulations [17]. It is found that the preferred conducting direction can be rotated by 90° with appropriate strain. The measured hall mobility for holes and the optical conductivity are anisotropic, experimentally [18]. BP absorbing less light energy polarized along the armchair direction than along the zigzag direction achieves a maximized optical conductivity in the armchair direction [9]. The peak of the anisotropic optical-absorption spectra is shifted towards the lower (higher) energy under compressive (tensile) strain [11]. Using the Kubo formula within an effective low-energy Hamiltonian, the optical conductivity tensor was

*Corresponding author: czhang@uow.edu.au

calculated, which is shown sensitively to the thickness and light polarization [19]. In a THz region, the optical intraband transitions contribute to the intraband optical conductivity in the vicinity of the Γ point which can be expressed by different in-plane effective electron masses along different directions [26–28]. In the presence of periodic stress, theoretical results predict that the optical-absorption band edge can be modified [20]. In the presence of two types of defects (i.e., short- and long-range defects), the anisotropy of defect-induced optical excitations is suppressed due to the isotropic nature of the defects [21]. BP exhibits in-plane anisotropic thermal conductivity with the preferential direction along the zigzag direction [22–24] which is different from the electric preferential direction along the armchair direction. The thermal energy transport in the supported and suspended BP sheets has been studied and found that supported BP exhibits an anomalous thermal anisotropy enhancement by coupling to the substrate [22]. The strain dependence of the thermal conductivity has also been discussed [23]. Using first-principles calculation and the nonequilibrium Green's-function method, Ong *et al.* investigated the ballistic thermal transport and the effect of strain on the thermal conductivity of BP [24]. They found that the thermal conductance is anisotropic and the orientation dependence can be tuned by the strain engineering.

In this paper, we investigate the angular dependent optical conductivity from intraband and interband optical transitions. Originating from the puckered lattice structure with nonplanar armchair and planar zigzag directions, it leads to an anisotropic optical conductivity. We shall demonstrate the anisotropic optical-absorption properties of BP under uniaxial and biaxial expansion or compression strains along the armchair and/or zigzag directions. To understand the properties of the optical conductivity, the dependence of the energy band structure on strain will be employed to analyze and discuss.

II. THEORETICAL APPROACHES

The tight-binding Hamiltonian for single layer pristine black phosphorene can be described as follows [21,29]:

$$H = \sum_{\nu,\nu'} t_{\nu,\nu'} c_\nu^\dagger c_{\nu'}, \tag{1}$$

where the summation runs over the lattice sites (ν,ν') of BP. $t_{\nu,\nu'}$ is the intralayer hopping energy between νth and ν'th sites. $c_\nu^\dagger$ $(c_{\nu'})$ is the creation (annihilation) operator of electrons at site ν (ν'). A unit cell of BP contains four phosphorus atoms, two puckered-up and two puckered-down atoms. In the momentum representation, the 4×4 Hamiltonian matrix reduces to a 2×2 matrix if puckered-up and puckered-down atoms are identical. The two-band Hamiltonian reads as

$$H_2 = \begin{pmatrix} f_{\mathbf{k}} & g_{\mathbf{k}} \\ g_{\mathbf{k}}^* & f_{\mathbf{k}} \end{pmatrix}. \tag{2}$$

Here, $f_{\mathbf{k}} = 4t_4\cos(k_x a/2)\cos(k_y b/2)$, $g_{\mathbf{k}} = 2t_1 e^{-ik_x a_{1x}}\cos(k_y b/2) + t_2 e^{ik_x a_{2x}} + 2t_3 e^{ik_x a_{3x}}\cos(k_y b/2) + t_5 e^{-ik_x a_{5x}} = |g_k| e^{i\theta_{\mathbf{k}}}$. $a_{1x} = 1.417\,63$ Å ($a_{2x} = 0.797\,32$ Å) is the distance between the intraplanar (interplanar) nearest-neighbor atoms projected to the x direction. $a_{3x} = a_{1x} + 2a_{2x}$, $a_{4x} = a_{1x} + a_{2x}$, $a_{5x} = 2a_{1x} + a_{2x}$. $a = 2(a_{1x} + a_{2x})$ and $b = 3.27$ Å are the lengths of the unit cell into the x direction (armchair) and y direction (zigzag). From Eq. (2), the conduction and valence energy bands can be obtained as

$$E_{\mathbf{k},s} = f_{\mathbf{k}} + s\sqrt{g_{\mathbf{k}} g_{\mathbf{k}}^*}. \tag{3}$$

The corresponding carrier states are

$$\psi_{\mathbf{k},s}(\mathbf{r}) = \frac{1}{\sqrt{2}}\begin{pmatrix} s e^{i\theta_{\mathbf{k}}} \\ 1 \end{pmatrix} e^{i\mathbf{k}\cdot\mathbf{r}}, \tag{4}$$

where $s = \pm1$ refers to the conduction band ($s = 1$) and the valence band ($s = -1$).

The bond lengths can be tuned by the strain engineering which leads to the modified hopping parameters. When an axial strain is applied, considering the relationship between the hopping energy and the bond length, $t \propto \frac{1}{r^2}$, in the linear deformation regime, the dependence of the hopping parameters on strain is given as

$$t_j/t_{0j} \approx 1 - 2(\alpha_{j,x}\varepsilon_x + \alpha_{j,y}\varepsilon_y + \alpha_{j,z}\varepsilon_z), \tag{5}$$

where t_j (t_{0j}) refers to the hopping energy in a distorted (undistorted) lattice. In Refs. [21] and [29], five hopping parameters are $t_{01} = -1.220$ eV, $t_{02} = 3.665$ eV, $t_{03} = -0.205$ eV, $t_{04} = -0.105$ eV, and $t_{05} = -0.055$ eV. ε_γ is the strain coefficient along the $\gamma = (x,y,z)$ direction. $\alpha_{j,\gamma} = r_{0j,\gamma}^2/r_{0j}^2$ are the coefficients relating to the structure of BP. $r_{0j,\gamma} = (x_{0j}, y_{0j}, z_{0j})$.

In the presence of the optical field $\mathbf{E}(\omega)$, the wave vector $\mathbf{k} \to \mathbf{k} + (e/\hbar)\mathbf{A}$ and the Hamiltonian becomes

$$H_2(\mathbf{A}) = \begin{pmatrix} f_{\mathbf{k}} + \Delta f_{\mathbf{k}}(\mathbf{A}) & g_{\mathbf{k}} + \Delta g_{\mathbf{k}}(\mathbf{A}) \\ g_{\mathbf{k}}^* + \Delta g_{\mathbf{k}}^*(\mathbf{A}) & f_{\mathbf{k}} + \Delta f_{\mathbf{k}}(\mathbf{A}) \end{pmatrix},$$

where $\mathbf{A} = \mathbf{E}/(i\omega)$ is the vector potential. Using the wave function in the absence of the optical field to construct electron quantum field operators in the $\mathbf{k}$ space, $\Psi(\mathbf{r}) = \sum_{\mathbf{k},s} c_{\mathbf{k},s}\psi(\mathbf{r})$ and $\Psi^\dagger(\mathbf{r}) = \sum_{\mathbf{k},s} c_{\mathbf{k},s}^\dagger \psi^*(\mathbf{r})$ where $c_{\mathbf{k},s}^\dagger$ and $c_{\mathbf{k},s}$ are the creation and annihilation operators for an electron at $(\mathbf{k},s)$ state. In the second quantized notation, the Hamiltonian can be written as $H = \sum_{\mathbf{k},s} E_{\mathbf{k},s} c_{\mathbf{k},s}^\dagger c_{\mathbf{k},s} + \mathbf{J}\cdot\mathbf{A}$. The components $J_{\mu=x,y}$ of the current operator $\mathbf{J}$ are

$$J_\mu = -\frac{e}{\hbar}\Sigma_{\mathbf{k},s} c_{\mathbf{k},s}^\dagger c_{\mathbf{k},s}\alpha_{\mathbf{k}}^\mu + i\frac{e}{\hbar}\Sigma_{\mathbf{k},s} c_{\mathbf{k},s}^\dagger c_{\mathbf{k},-s}\beta_{\mathbf{k}}^\mu, \tag{6}$$

where $u = x$ or y, $\alpha_{\mathbf{k}}^x = 2t_4 a\sin(k_x a/2)\cos(k_y b/2) + 2t_1 a_{1x}\cos(k_y b/2)\sin(k_x a_{1x} + \theta_{\mathbf{k}}) + t_2 a_{2x}\sin(k_x a_{2x} - \theta_{\mathbf{k}}) + 2t_3 a_{3x}\cos(k_y b/2)\sin(k_x a_{3x} - \theta_{\mathbf{k}}) + t_5 a_{5x}\sin(k_x a_{5x} + \theta_{\mathbf{k}})$, $\beta_{\mathbf{k}}^x = -2t_1 a_{1x}\cos(k_y b/2)\cos(k_x a_{1x} + \theta_{\mathbf{k}}) + t_2 a_{2x}\cos(k_x a_{2x} - \theta_{\mathbf{k}}) + 2t_3 a_{3x}\cos(k_y b/2)\cos(k_x a_{3x} - \theta_{\mathbf{k}}) - t_5 a_{5x}\cos(k_x a_{5x} + \theta_{\mathbf{k}})$, $\alpha_{\mathbf{k}}^y = 2t_4 b\cos(k_x a/2)\sin(k_y b/2) + b\sin(k_y b/2)[t_1\cos(k_x a_{1x} + \theta_{\mathbf{k}}) + t_3\cos(k_x a_{3x} - \theta_{\mathbf{k}})]$, $\beta_{\mathbf{k}}^y = b\sin(k_y b/2)[t_1\sin(k_x a_{1x} + \theta_{\mathbf{k}}) - t_3\sin(k_x a_{3x} - \theta_{\mathbf{k}})]$. Using the Kubo formula, the optical conductivity is given as

$$\sigma_{\mu,\mu'} = \frac{g_s}{\hbar\omega S}\int_0^\infty dt e^{i\omega t}\langle[j_\mu(t), j_{\mu'}(0)]\rangle, \tag{7}$$

where $g_s = 2$ is the spin degeneracy. S is the 2D planar area. The intraband transitions (s,s) contribute to the optical conductivity in the presence of the disorder or scattering in the THz region which can be described as the Drude-like conductivity,

$$\sigma_{\mu,\mu}^{\text{intra}} = i\frac{g_s\sigma_0}{\pi^2(\hbar\omega + i\delta_1)}\int_0^{\pi/a}\frac{\left(\alpha_{\mathbf{k}}^\mu\right)^2}{|\partial E_{\mathbf{k},+}/\partial k_y|_{k_{F,y}}}dk_x. \tag{8}$$

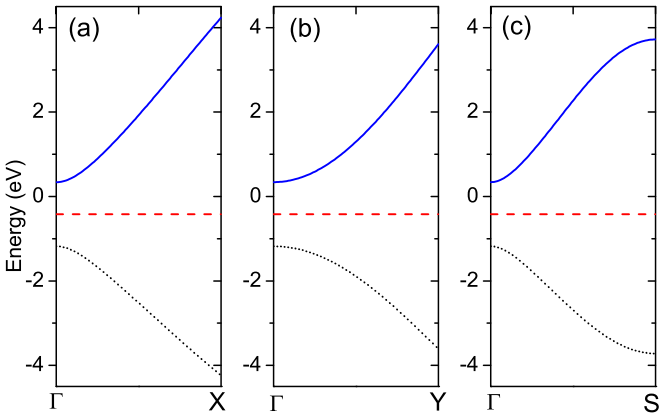

FIG. 1. The band structure of single layer BP in the absence of strain along $\Gamma - X$ (a), $\Gamma - Y$ (b), $\Gamma - S$ (c) directions. Γ, X, Y, and S are (0,0), $(\pi/a,0)$, $(0,\pi/b)$, and $(\pi/a,\pi/b)$ points in a (k_x,k_y) Brillouin zone. Red dashed lines represent the energy in the midpoint between the valence band (black dotted line) and the conduction band (blue solid line) at Γ point.

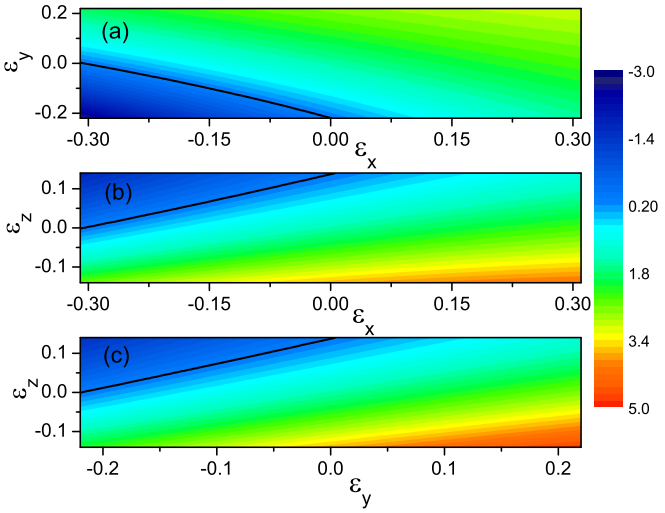

FIG. 2. The energy gap at Γ point under biaxial strains, with strains applied along (x,y) (a), (x,z) (b), and (y,z) (c) directions. The color bar represents the energy gap value. The unit is eV. The black solid lines represent the zero energy gap.

$\sigma_0 = e^2/\hbar$, δ_1 is the broadening width determined by scattering or disorder in the conduction band. $k_{F,y}$ depends on the integration parameter k_x which satisfies $E(k_{F,y},k_x) = E_F$.

When the incident optical energy is large enough, the carriers absorb this energy and transmit from the valence band to the conduction band. The longitudinal optical conductivity from the interband transitions $(s, -s)$ has been obtained as

$$\sigma^{\text{inter}}_{\mu,\mu} = i\zeta \sum_{\mathbf{k}} \left(\beta^{\mu}_{\mathbf{k}}\right)^2 \left[\frac{f_{\mathbf{k},+} - f_{\mathbf{k},-}}{\hbar\omega + \Delta E_{\mathbf{k}} + i\delta_2} - \frac{f_{\mathbf{k},+} - f_{\mathbf{k},-}}{\hbar\omega - \Delta E_{\mathbf{k}} + i\delta_2}\right]. \tag{9}$$

Here, $\zeta = g_s\sigma_0/(\hbar\omega S)$. $\Delta E_{\mathbf{k}} = (E_{\mathbf{k},+} - E_{\mathbf{k},-})$. $f_{\mathbf{k},s}$ is the Dirac-Fermi distribution function. δ_2 accounts for the finite damping between the conduction band and the valence band. The interband optical conductivity relates to the energy difference between two bands. In addition, the Hall optical conductivity $\sigma_{x,y} = \sigma_{y,x} = 0$ because of the structure symmetry. In the following, the strain effect on the optical conductivity will be investigated.

III. RESULTS AND DISCUSSIONS

The calculated band dispersion for single layer BP in the absence of strain is shown in Fig. 1. The energy dispersion is anisotropic. The energy gap is $E_g = 4(t_1 + t_3) + 2(t_2 + t_5) = 1.52$ eV which depends on the hopping energies t_1, t_2, t_3, and t_5. In the presence of tensile and/or compressive strains, the lengths r_{0j} between the nearest-neighbor and next-nearest-neighbor atoms become r_j which leads to all these hopping parameters being tuned. The energy gap as a function of biaxial strain is depicted in Fig. 2. The main coupling parameters are t_1 and t_2 from the nearest-neighbor atoms. Therefore, we focus our discussion on the modifications of r_1 and r_2 when strain is applied in different directions. When a tensile strain is along the x direction, according to the relationship of $r_{j,\gamma} = (1 + \varepsilon_\gamma)r_{0j,\gamma}$ both r_1 and r_2 become longer. Using Eq. (5), the absolute values of the related hopping parameters become smaller because of the coefficient $\alpha_{1/2,x} > 0$. If the tensile strain is along the y direction, only r_1 is elongated, while $r_2 = r_{02}$ remains unchanged because of $\alpha_{2,y} = 0$. If the tensile strain is applied in the z direction, only r_2 is elongated and $r_1 = r_{01}$ remains unchanged because of $\alpha_{1,z} = 0$. It is noted that t_2 is positive while other hopping parameters are negative. Considering the relationship $t/t_0 = (r/r_0)^{-2}$, the simulation results for the energy gap can be concluded in Fig. 2. The band gap of BP increases when increasing the strain along the x/y axis. But the strain effect along the z axis on the energy gap exhibits in an opposite way. With the same uniaxial strain value, the effect of ε_z strain on the energy gap is stronger than that of ε_y strain. The effect of ε_x strain on the energy dispersion is weaker than that of the ε_y and ε_z strains. At a critical strain value, the energy gap becomes zero which is represented by black solid lines in Fig. 2. Increasing or decreasing the strain further along different directions leads to the occurrence of the negative band gap, shown in Fig. 2. Figure 3 illustrates the energy difference between the conduction band and the valence band $(E_+ - E_-)$ along the (k_x,k_y) Brillouin plane. This energy difference is symmetric about the k_x and k_y axes, but anisotropic along other different axes which can be tuned by the applied tensile and compressive strains. The compressive strain applied in the z direction has an obvious influence on this energy difference. When an optical field is present, the carriers absorb optical energy and make a transition from the valence band to the conduction band vertically to satisfy the energy and momentum conservations which relate to this energy difference at the same wave vector.

We now discuss the intraband and interband optical conductivity and the dependence on the uniaxial and biaxial strains in BP. In the THz frequency region, the main contributions to the optical conductivity are from the intraband optical transitions $(\mathbf{q} \to 0)$ where $\mathbf{q}$ indicates the wave-vector change before and after the scattering process. Figure 4 illustrates the real and imaginary parts of the intraband optical conductivity versus the incident optical energy at different chemical potential

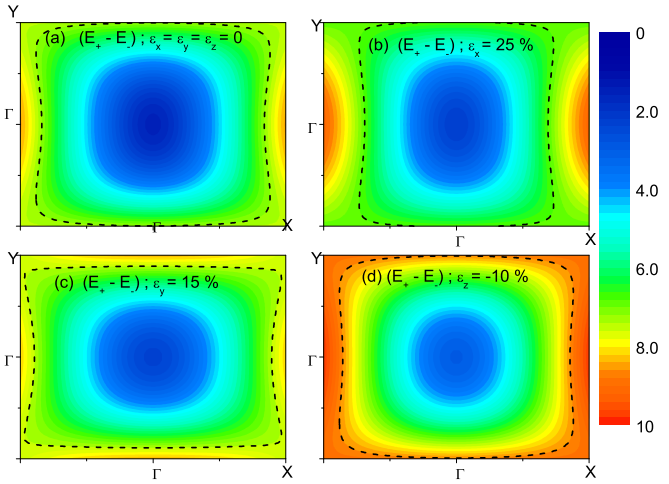

FIG. 3. The energy difference between the conduction band (E_+) and the valence band (E_-) in the absence of strain (a), under uniaxial tensile strain $\epsilon_x = 25\%$ (b), $\epsilon_y = 15\%$ (c), and compressive strain $\epsilon_z = -10\%$ (d). The black dashed lines represent the maximum continuous equal energy line in a Brillouin zone. The color bar represents the energy difference value. The unit is eV.

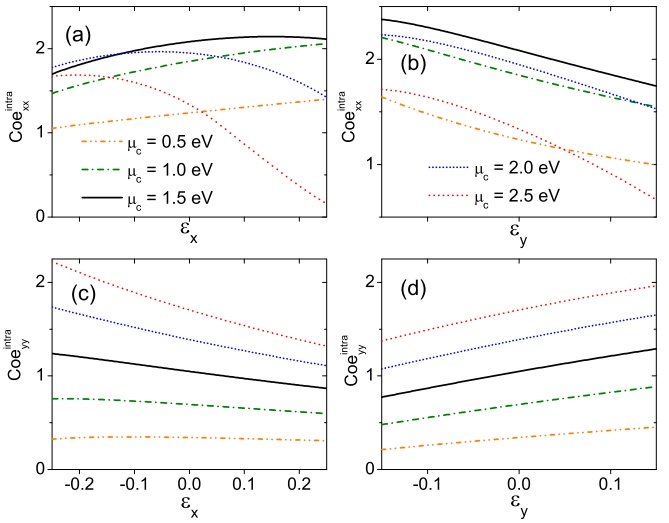

FIG. 5. The coefficients of the intraband optical conductivities along the armchair ($\mathrm{Coe}_{xx}^{\mathrm{intra}}$) and zigzag ($\mathrm{Coe}_{yy}^{\mathrm{intra}}$) directions with strain applied along the x (a),(b) and y (c),(d) directions at different chemical potential μ_c.

$\mu_c = 0.5, 1, 1.5, 2, 2.5$ eV in the absence of strain. This Drude-like intraband optical conductivity along the armchair (x) and zigzag (y) directions exhibits anisotropic characteristics. The x component of the conductivity is larger than the y component which presents the preferential conducting direction being the armchair direction. In Ref. [26], using two anisotropic effective masses around the Γ point, the Drude conductivity was inversely proportional to these masses and the obtained σ_{xx} is larger than σ_{yy} theoretically. Increasing the chemical potential, the optical conductivity $\sigma_{yy}^{\mathrm{intra}}$ increases while $\sigma_{xx}^{\mathrm{intra}}$ increases at first and decreases later which can be traced to the total effect of the carriers' motions. When the electric field is applied along the armchair direction, the main interactions t_1 and t_2 cause carriers to move in an opposite direction which makes the dependence of $\sigma_{xx}^{\mathrm{intra}}$ on the chemical potential and the strain complicated. The intraband optical conductivity is determined by the Drude coefficient from the wave-vector integration $\mathrm{Coe}_{\mu\mu}^{\mathrm{intra}} = \int_0^{\pi/a} \frac{(\alpha_{\mathbf{k}}^{\mu})^2}{|\partial E_{\mathbf{k},+}/\partial k_y|_{k_{F,y}}} dk_x$ in Eq. (8), and the dependence on ε_x and ε_y has been plotted in Fig. 5. With the increase of ε_x and ε_y, the integration coefficient of the wave vector $\mathrm{Coe}_{yy}^{\mathrm{intra}}$ monotonically decreases and increases which can be seen in Figs. 5(c) and 5(d). Along the armchair direction, when the chemical potential is lower than about 1.0 eV, the integration coefficient monotonically increases and decreases with the increase of ε_x and ε_y [see Figs. 5(a) and 5(b)]. After continuing to increase the chemical potential over a critical value (about 1.5 eV), the dependence of $\mathrm{Coe}_{xx}^{\mathrm{intra}}$ on strain is complicated.

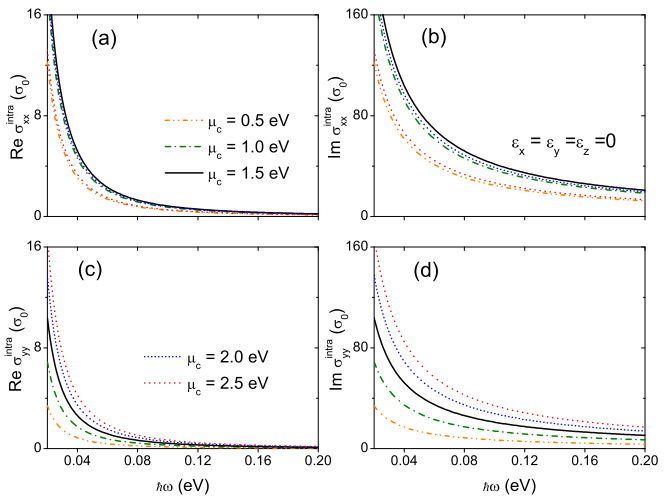

FIG. 4. The real (a),(c) and imaginary (b),(d) parts of the intraband optical conductivities along the armchair $\sigma_{xx}^{\mathrm{intra}}$ and zigzag $\sigma_{yy}^{\mathrm{intra}}$ directions as a function of the optical energy at different chemical potential μ_c in the absence of strain. $E_F = E_c(\Gamma) + \mu_c$. Conductivities are normalized with respect to $\sigma_0 = e^2/\hbar$.

In the interband optical transition calculation, the Fermi energy E_F is located at the midgap between the valence band and the conduction band at the Γ point and the damping term $\delta_2 = 0.08$. Figures 6 and 7 show the real and imaginary parts of the optical conductivity $\sigma_{xx}^{\mathrm{inter}}$ and $\sigma_{yy}^{\mathrm{inter}}$ versus the incident optical energy. The profiles of the interband optical conductivity for the incident light polarized along the armchair ($\sigma_{xx}^{\mathrm{inter}}$) and zigzag ($\sigma_{yy}^{\mathrm{inter}}$) directions are strongly asymmetric which is the result of the anisotropic energy-band structure. In the presence of uniaxial strain, the change of energy gap can be directly observed from the shift of the $\mathrm{Re}\sigma_{xx}^{\mathrm{inter}}$ peak. However the peak height of $\mathrm{Re}\sigma_{xx}^{\mathrm{inter}}$ under different uniaxial strain ε_x remains roughly unchanged. At frequencies larger than the absorption edge, $\mathrm{Re}\sigma_{xx}^{\mathrm{inter}}$ decreases with the increase of the optical energy. At a certain high frequency, $\mathrm{Re}\sigma_{xx}^{\mathrm{inter}}$ decreases drastically which corresponds to the maximum continuous equal energy difference in the Brillouin zone in Fig. 3. When the equal energy line in a reciprocal space is continuous, it can provide sufficient channels for carriers in the valence band absorbing optical energy and transmitting to the conduction

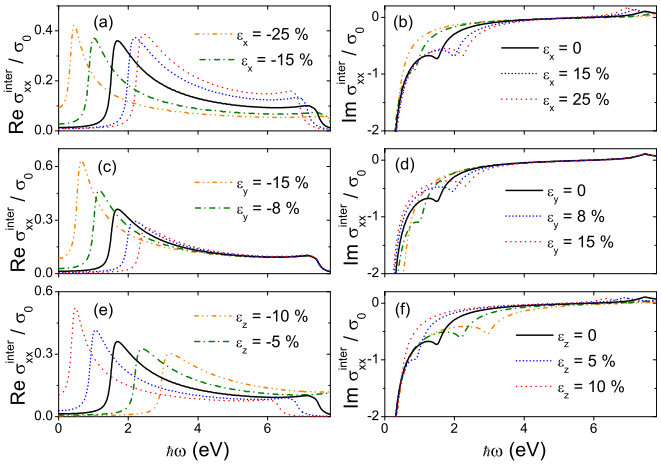

FIG. 6. The real (a),(c),(e) and imaginary (b),(d),(f) parts of the interband optical conductivities $\sigma_{xx}^{\text{inter}}$ vs the optical energy at different uniaxial tensile and compressive strains, with strain applied along the x (a),(b), y (c),(d), and z (e),(f) directions.

band. If this maximum continuous energy line is too high which indicates the high incident optical energy, the two-band Hamiltonian becomes inaccurate and more bands should be included in the model. In the two-band model, the characteristics of the interband optical conductivity polarized along the armchair direction drastically decreasing at the high-energy region will be glossed over. From Figs. 6(b), 6(d), and 6(f), the value of the imaginary part of the optical conductivity $\text{Im}\sigma_{xx}^{\text{inter}}$ can be negative or positive. The dip position in the low frequency in $\text{Im}\sigma_{xx}^{\text{inter}}$ reflects the band gap. The interband optical conductivity polarized along the zigzag direction $\sigma_{yy}^{\text{inter}}$ increases with increasing the optical energy to the above-mentioned critical energy difference. Another interesting phenomenon is that the effect of the strain ε_z on the optical conductivity is opposite to that when the strain is along the x and y directions. In the presence of biaxial strains, the energy spectrum can be efficiently modulated. Therefore, the optical conductivity depends on biaxial strains which can be observed in Fig. 8. The main features about the dependence on the optical

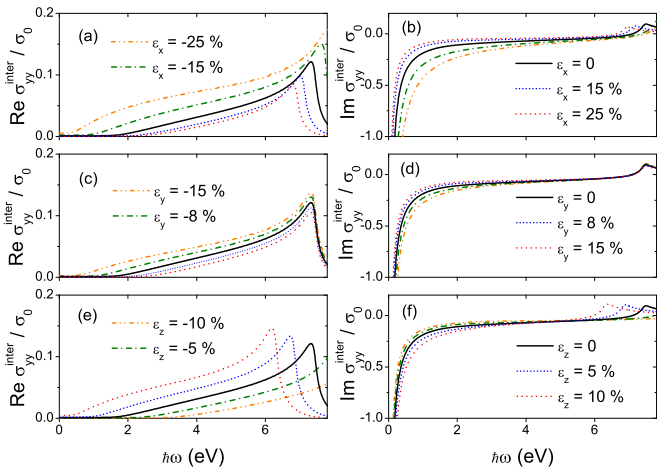

FIG. 7. Same as Fig. 6 except for the interband optical conductivity $\sigma_{yy}^{\text{inter}}$.

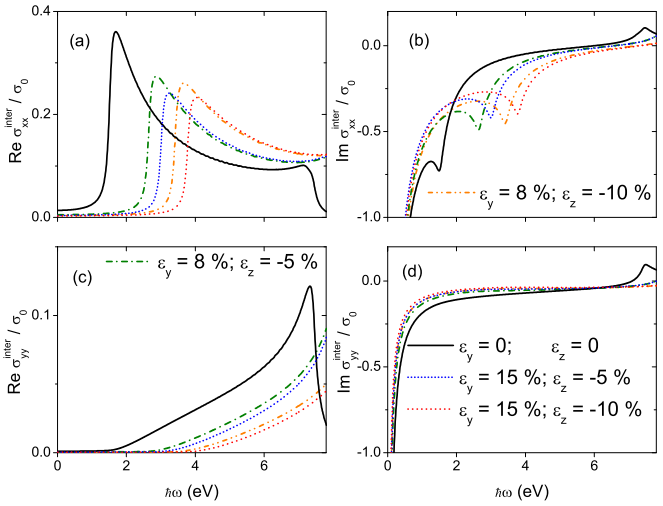

FIG. 8. The real (a),(c) and imaginary (b),(d) parts of the interband optical conductivities $\sigma_{xx}^{\text{inter}}$ (a),(b) and $\sigma_{yy}^{\text{inter}}$ (c),(d) as a function of biaxial tensile and compressive strains along (y,z) directions.

frequency and strain have been retained. But compared with the effect of uniaxial strain on σ^{inter}, smaller biaxial strains will achieve the same optical conductivity value. Figure 9 plots the total BP optical conductivity at different chemical potential in the conduction band in the absence of strain. Here, the temperature was set at 10 K. The main contributions from intraband and interband optical transition processes locate in the low and high incident optical energy region, respectively. The optical energy of the peak position in $\text{Re}\sigma_{xx}$ corresponds to $E_g + 2\mu_c$. When $\mu_c = 0.5$ eV, the total imaginary part of $\text{Im}\sigma_{xx}$ is positive which can be applied in the transverse magnetic (TM) surface plasmon propagation. Decreasing the chemical potential to 0.1 eV, $\text{Im}\sigma_{xx}$ exhibits negative at about $E_g + 2\mu_c$ which is similar to the 2D monolayer graphene

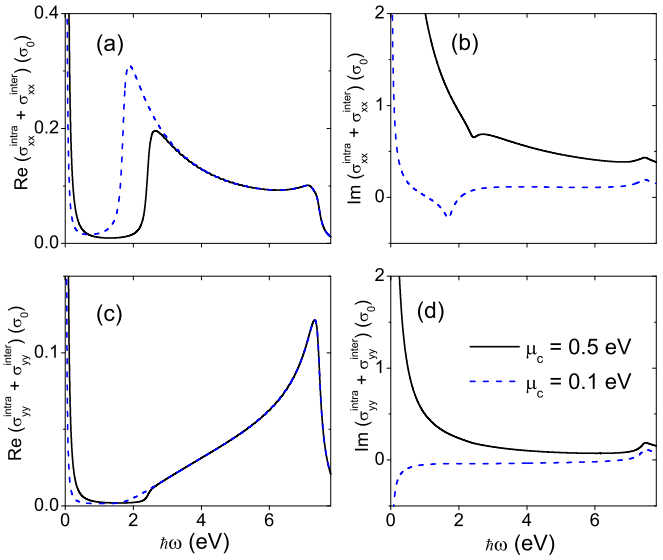

FIG. 9. The real (a),(c) and imaginary (b),(d) parts of the total optical conductivities along the armchair direction (x) (a),(b) and along the zigzag direction (y) (c),(d) vs the incident optical energy.

material and can support the transverse electric (TE) surface plasmon propagation [30,31].

In summary, in a 2D nonplanar BP both the energy-band structure and the optical conductivity exhibit strong anisotropy which can be modified by uniaxial and biaxial tensile and compressive strains. The modulation under biaxial strain is more effective than that under uniaxial strain. The energy gap increases with the strain applied along the x and y directions increasing. But the dependence of the energy gap on the z direction strain is opposite to the other two direction strains. In the presence of the optical field, it will make carriers transmit among the conduction band or from the valence band to the conduction band which contributes to the BP's intraband and interband optical conductivity. The intraband optical conductivity polarized along the zigzag direction exhibits monotonically dependence on the Fermi energy and strain. However, along the armchair direction the complex dependence was observed which originates from the competitive carriers' motions from t_1 and t_2 interaction. The blueshifts and redshifts of the absorption edge in the interband optical conductivity polarized along the armchair direction can be observed and the energy gap can be obtained in the presence of different strains. Above the energy gap, increasing the incident optical energy the real part of the optical conductivity $\mathrm{Re}\sigma_{xx}^{\mathrm{inter}}$ ($\mathrm{Re}\sigma_{yy}^{\mathrm{inter}}$) decreases (increases). When the optical energy increases to a critical value, the absorption drops abruptly. It is found that the total imaginary part of the BP optical conductivity can be modified by the chemical potential. This property can be used to study the dispersion and propagation properties of TE/TM surface plasmon.

ACKNOWLEDGMENTS

This work was supported by the China Scholarship Council, the Natural Science Foundation of Jiangsu Province (Grant No. BK20131428), and the National Science Foundation of China (Grant No. 11547030).

[1] H. Liu, A. T. Neal, Z. Zhu, Z. Luo, X. Xu, D. Tománek, and P. D. Ye, ACS Nano **8**, 4033 (2014).
[2] L. Li, Y. Yu, G. J. Ye, Q. Ge, X. Ou, H. Wu, D. Feng, X. H. Chen, and Y. Zhang, Nat. Nanotechnol. **9**, 372 (2014).
[3] M. Ashton, J. Paul, S. B. Sinnott, and R. G. Hennig, Phys. Rev. Lett. **118**, 106101 (2017).
[4] A. Castellanos-Gomez, J. Phys. Chem. Lett. **6**, 4280 (2015).
[5] H. Liu, Y. Du, Y. Deng, and P. D. Ye, Chem. Soc. Rev. **44**, 2732 (2015).
[6] E. T. Sisakht, M. H. Zare, and F. Fazileh, Phys. Rev. B **91**, 085409 (2015).
[7] A. N. Rudenko and M. I. Katsnelson, Phys. Rev. B **89**, 201408(R) (2014).
[8] V. Tran, R. Soklaski, Y. Liang, and L. Yang, Phys. Rev. B **89**, 235319 (2014).
[9] G. Zhang, S. Huang, A. Chaves, C. Song, V. O. Özçelik, T. Low, and H. Yan, Nat. Commun. **8**, 14071 (2017).
[10] D. Çakır, C. Sevik, and F. M. Peeters, Phys. Rev. B **92**, 165406 (2015).
[11] D. Çakır, H. Sahin, and F. M. Peeters, Phys. Rev. B **90**, 205421 (2014).
[12] J.-W. Jiang and H. S. Park, Phys. Rev. B **91**, 235118 (2015).
[13] B. Sa, Y.-L. Li, J. Qi, R. Ahuja, and Z. Sun, J. Phys. Chem. C **118**, 26560 (2014).
[14] S. S. Baik, K. S. Kim, Y. Yi, and H. J. Choi, Nano Lett. **15**, 7788 (2015).
[15] J. Kim, S. S. Baik, S. H. Ryu, Y. Sohn, S. Park, B.-G. Park, J. Denlinger, Y. Yi, H. J. Choi, and K. S. Kim, Science **349**, 723 (2015).
[16] S. Ono, J. Appl. Phys. **121**, 204301 (2017).
[17] R. Fei and L. Yang, Nano Lett. **14**, 2884 (2014).
[18] F. Xia, H. Wang, and Y. Jia, Nat. Commun. **5**, 4458 (2014).
[19] T. Low, A. S. Rodin, A. Carvalho, Y. Jiang, H. Wang, F. Xia, and A. H. C. Neto, Phys. Rev. B **90**, 075434 (2014).
[20] J. Quereda, P. San-Jose, V. Parente, L. Vaquero-Garzon, A. J. Molina-Mendoza, N. Agraït, G. Rubio-Bollinger, F. Guinea, R. Roldàn, and A. Castellanos-Gomez, Nano Lett. **16**, 2931 (2016).
[21] S. Yuan, A. N. Rudenko, and M. I. Katsnelson, Phys. Rev. B **91**, 115436 (2015).
[22] J. Chen, S. Chen, and Y. Gao, J. Phys. Chem. Lett. **7**, 2518 (2016).
[23] A. Jain and A. J. H. McGaughey, Sci. Rep. **5**, 8501 (2015).
[24] Z.-Y. Ong, Y. Cai, G. Zhang, and Y.-W. Zhang, J. Phys. Chem. C **118**, 25272 (2014).
[25] J.-W. Jiang and H. S. Park, Nat. Commun. **5**, 4727 (2014).
[26] T. Low, R. Roldán, H. Wang, F. Xia, P. Avouris, L. M. Moreno, and F. Guinea, Phys. Rev. Lett. **113**, 106802 (2014).
[27] Z. Liu and K. Aydin, Nano. Lett. **16**, 3457 (2016).
[28] D. Correas-Serrano, J. S. Gomez-Diaz, A. A. Melcon, and A. Alù, J. Opt. **18**, 104006 (2016).
[29] M. Ezawa, New J. Phys. **16**, 115004 (2014).
[30] S. A. Mikhailov and K. Ziegler, Phys. Rev. Lett. **99**, 016803 (2007).
[31] X. Luo, T. Qiu, W. Lu, and Z. Ni, Mater. Sci. Eng., R **74**, 351 (2013).